# Electrocatalytic Reduction of CO_2 with Palladium Bis-N-heterocyclic Carbene Pincer Complexes

Jeffrey A. Therrien, Michael O. Wolf,* and Brian O. Patrick

Department of Chemistry, University of British Columbia, Vancouver, British Columbia V6T 1Z1, Canada

Ⓢ Supporting Information

ABSTRACT: A series of pyridine- and lutidine-linked bis-N-heterocyclic carbene (NHC) palladium pincer complexes were electrochemically characterized and screened for CO_2 reduction capability with 2,2,2-trifluoroethanol, acetic acid, or 2,2,2-trifluoro-acetic acid (TFA) as proton sources. The lutidine-linked pincer complexes electrocatalytically reduce CO_2 to CO at potentials as low as -1.6 V versus $Ag/AgNO_3$ in the presence of TFA. The one-electron reduction of these complexes is shown to be chemically reversible, yielding a monometallic species, with density functional theory studies indicating charge storage on the redox-active ligand, thus addressing a major source of deactivation in earlier triphosphine electrocatalysts.
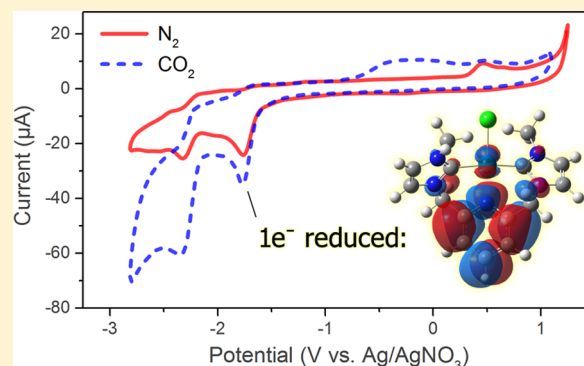
INTRODUCTION

Interest in CO_2 reduction catalysis has increased drastically over the last two decades as researchers are responding to the steady increase in atmospheric CO_2 from anthropogenic sources and the need for renewable and sustainable energy sources.[1,2] Current technologies allow electrical energy to be stored in batteries and capacitors. Hydrocarbon fuels, however, have a significantly higher energy density than current or projected battery technologies and have many important applications that will not soon be replaced.[3] Additionally, much of the world's energy infrastructure is already based on hydrocarbon fuels. Efficiently generating "solar fuels," that is, CO_2-derived fuels using renewable energy sources, can in principle enable a carbon-neutral fuel cycle.[3]

The reduction of CO_2 to liquid fuels precursors (CO + H_2, synthesis gas)[4,5] or directly to liquid fuels (such as methanol or methane) is thermodynamically feasible with these reactions becoming increasingly favorable concomitant with an increasing number of proton-coupled electrons transferred. The thermodynamic potentials for relevant reduction products are given in Table 1. Performing these reactions near their thermodynamic potentials is challenging, however, requiring the use of catalysts to minimize the energy barriers of CO_2 activation and allow or facilitate subsequent proton transfers.

Recent research into homogeneous CO_2 reduction catalysts has largely focused on variations of established families of catalysts such as group 7 bipyridine tricarbonyl complexes[7–10] and porphyrin, salen, and other planar tetracoordinate ligand systems on Fe and Ni[11–13] to produce the two-electron reduction product CO. A robust understanding of the underlying mechanisms and structure–activity relationships for CO_2 reduction (especially for higher reduction products) is growing,

Table 1. Thermodynamic Potentials of CO_2 and H^+ Reduction Products at pH 7[6]

half-reaction	potential vs SCE (V)
$CO_2 + e^- \rightarrow CO_2^{\bullet-}$	$E° = -2.14$
$CO_2 + 2H^+ + 2e^- \rightarrow HCO_2H$	$E° = -0.85$
$CO_2 + 2H^+ + 2e^- \rightarrow CO + H_2O$	$E° = -0.77$
$CO_2 + 4H^+ + 4e^- \rightarrow CH_2O + H_2O$	$E° = -0.72$
$CO_2 + 6H^+ + 6e^- \rightarrow CH_3OH + H_2O$	$E° = -0.62$
$CO_2 + 8H^+ + 8e^- \rightarrow CH_4 + 2H_2O$	$E° = -0.48$
$2H^+ + 2e^- \rightarrow H_2$	$E° = -0.66$

in part due to the application of computational methods,[14,15] but is still embryonic.

The development of another class of homogeneous CO_2-reduction electrocatalysts, Pd phosphine-containing pincer catalysts, has been pursued almost exclusively by DuBois and co-workers,[2,16−19] following the earlier discovery of a Rh phosphine electrocatalyst by Wagenknecht et al. in 1984.[20] Various $[Pd(L_3)(CH_3CN)](BF_4)_2$ complexes were found to be efficient and selective electrocatalysts for the reduction of CO_2 to CO in acidic dimethylformamide (DMF) and CH_3CN, exhibiting Faradaic efficiencies >95% and operating at low potentials.[2,16,21] Catalyst turnover numbers (TON) were relatively small at only 10−200, however, due to the formation of an inert bimetallic species through Pd(I)−Pd(I) bonding and ligand bridging (which can be reversed by oxidation of the

bimetallic species). Both the mechanism and structure–activity relationships were elucidated for CO formation in these catalysts, and it was shown that CO_2 coordinates to the axial position of the reduced complexes.[21] It was also discovered that a bimetallic version of the catalyst exhibited a reaction rate 3 orders of magnitude higher than the monometallic complex due to cooperative effects, operating at rates comparable to the CO dehydrogenase enzyme, though with a very low TON (8).[18]

In an effort to further explore the pincer motif for CO_2-reduction electrocatalysts, we report here our investigation of other strongly electron-donating pincer complexes, specifically, those incorporating N-heterocyclic carbene (NHC) moieties as they are well-known to behave analogously to phosphines.[22,23] It was reasoned that pincer complexes of this general type may provide storage of redox equivalents away from the metal center akin to the function of the bipyridine ligand in Re(bpy)(CO)3X electrocatalysts,[1,4,24] which, combined with nonlabile M-NHC bonds, could improve TON relative to complexes containing phosphine ligands. Additionally, NHC and pyridyl containing ligands have recently been used in other designs of CO_2 reduction electrocatalysts.[10,12] Group 10 pyridyl-bridged bis-NHC pincer complexes have been previously synthesized and tested for carbon–carbon bond-formation catalysis, but without consideration as potential electrocatalysts. Here, a series of pyridyl-bridged and lutidine-bridged bis-NHC palladium complexes, **1–4**, are reported. Electrochemical characterization and screening for electrocatalytic CO_2 reduction ability, as well as density functional theory (DFT) computations and comparisons to other known electrocatalysts are discussed.

1, [Pd(C^N^C)Cl]BF4   **2, [Pd(bC^N^bC)Cl]BF4**

3, [Pd(C-N-C)Br]Br   **4, [Pd(bC-N-bC)Br]Br**
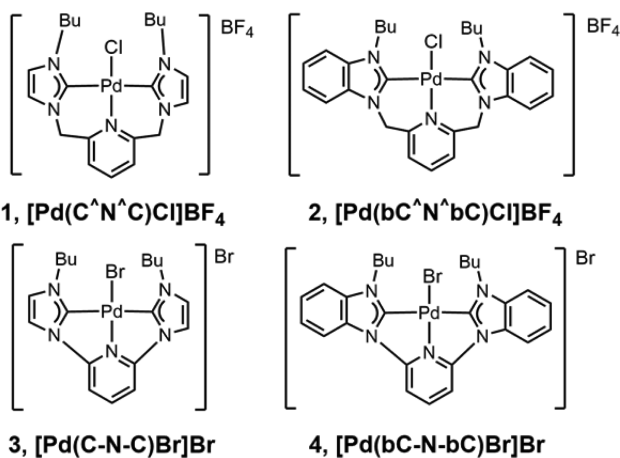
■ RESULTS AND DISCUSSION

The complexes under study varied by bridge type (lutidine, **1** and **2**, or pyridine, **3** and **4**) and NHC-donor type (imidazolilydene, **1** and **3**, or benzimidazolilydene, **2** and **4**). Two literature approaches were employed for their synthesis: namely, (i) protonolysis of the proligand with palladium acetate at high temperatures in a microwave reactor[25,26] and (ii) formation of silver carbene species from the proligand and subsequent transmetalation to dichloro(1,5-cyclooctadiene)palladium.[27,28] The transmetalation approach afforded **1** and **2** in higher purity (Supporting Information, Figures S1 and S2). Methods of purifying the protonolysis product mixtures by column chromatography on SiO_2 with KNO_3(aq) in the acetonitrile eluent were also developed and utilized, affording comparable purity to the silver carbene transmetalation product as determined by NMR analysis. Complexes **3** and **4** were obtained

without need for further purification via protonolysis at 160 °C in a microwave reactor and subsequent precipitations from addition of a dichloromethane solution to diethyl ether (Supporting Information, Figures S3 and S4). Complexes **1–4** are all thermally-, air-, and moisture-stable.[25,27,28]

Electrochemical Characterization. The complexes were characterized by cyclic voltammetry under both N_2 and CO_2 atmospheres. Under N_2, the lutidine-bridged complexes **1** and **2** exhibited similar behavior with two irreversible cathodic waves observed at peak potentials of −1.73 and −2.28 V for **1** and −1.65 and −2.13 V for **2** (Figure 1 and Supporting Information, Figure S5). Using controlled potential electrolysis at a potential approximately 150 mV more negative than the first cathodic wave, it was determined that the first reduction wave is a one-electron transfer process (0.89 F/mol for **1** and 0.91 F/mol for **2**).

As the electrolysis proceeded, a color change in the solution from very pale yellow to golden yellow was observed, and a new anodic wave emerged at 0.50 V for **1** and 0.57 V for **2**. These new waves have similar peak currents to the original cathodic waves, indicating the production of a relatively stable reduced species. The wave at 0.50 V for complex **1** became two overlapping waves at 0.47 and 0.61 V after electrolysis over a time period of 15 min, whereas the reduced species of **2** maintained one wave at 0.57 V. Exhaustive oxidation at these potentials led to re-emergence of the originally reduced cathodic wave, indicating a chemically reversible process (Figure 2). In both cases, the second cathodic wave was not affected by the one-electron transfer reaction. A one-electron transfer event is desirable as concurrent one-electron transfers can be beneficial to selectively reduce CO_2 in the presence of H^+ ions.[16,29]

The pyridyl-bridged complexes **3** and **4** show different electrochemical behavior than **1** and **2** (Figure 3). Complex **3** exhibits three irreversible cathodic waves of decreasing intensity at −1.60, −1.92, and −2.20 V, and **4** has two cathodic waves at −1.38 and −1.76 V and a third diminished wave at −2.13 V (Supporting Information, Figure S6). Both display an anodic wave at +0.33 V due to oxidation of the free bromide counterion present in solution. The peak current of the first cathodic wave in both complexes **3** and **4** is approximately 85−90% that of the peak current for the oxidation of the bromide counterion, indicating that the cathodic waves are one-electron reductions. A slightly greater relative peak current for the bromide oxidation wave is expected as the smaller anion will have a higher diffusion rate than the larger cationic complex according to the Stokes−Einstein equation. Exhaustive controlled potential electrolysis of complex **3** at −1.75 V was unsuccessful as the passage of current diminished within minutes due to the formation of a black, insulating solid on the electrode surface. The decomposition of **3** into an insulating solid may also cause the decreasing peak current as the complex undergoes successive reductions, as clearly seen in the square wave voltammogram of **3** (Supporting Information, Figure S6). Likewise, the diminished current for the cathodic wave at −2.13 V with **4** may be due to decomposition as well, where the increased π-conjugation in **4** is better able to stabilize the singly reduced complex than in **3**, but is still unable to stabilize the doubly reduced complex. Nevertheless, each of the cathodic waves for these species can be assigned as one-electron reductions by comparison to the bromide oxidation wave.

For complexes **1–4**, all of the cathodic waves remained electrochemically irreversible up to a scan rate of 1000 mV/s. Plots of peak current against the square root of the scan rate are
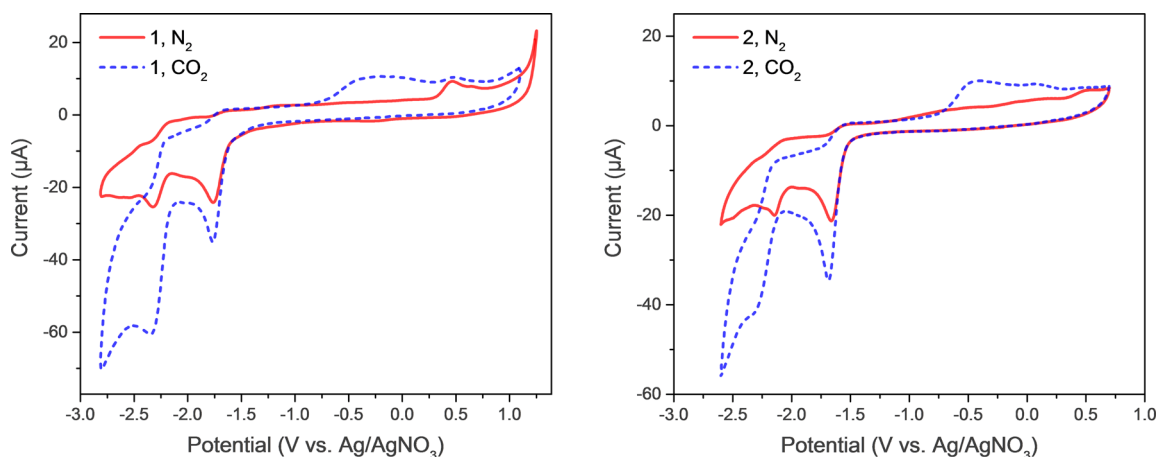
Figure 1. Cyclic voltammograms of **1** (left) and **2** (right) under N_2 and CO_2. CVs were recorded at 100 mV/s for 2 mM solutions of the complex in 0.1 M TBAPF$_6$/DMF.
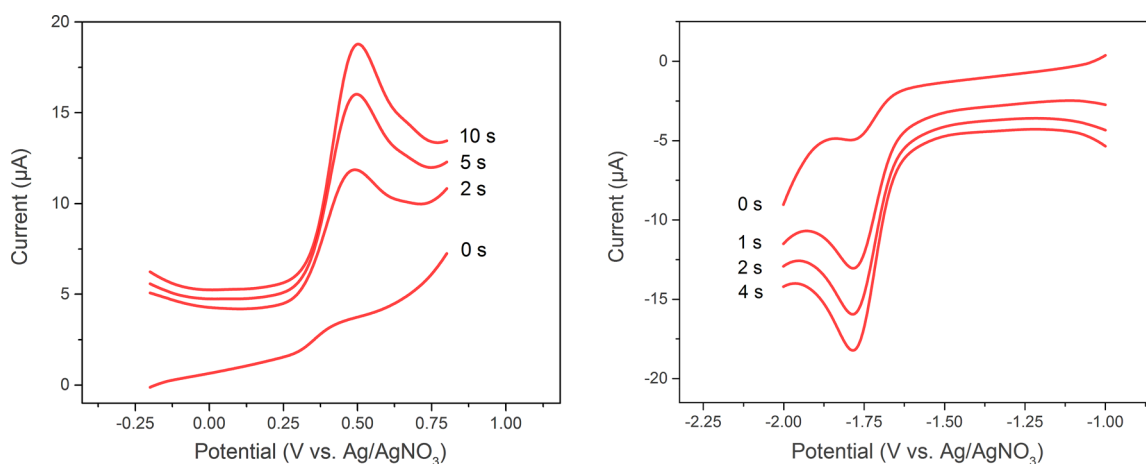

Figure 2. Square wave voltammograms of **1** after reduction at the peak potential of the first cathodic wave for varying amounts of time (left) and the one-electron reduced product of **1** after oxidation at the potential of the produced anodic wave for varying amounts of time (right) showing chemical reversibility of the redox process.
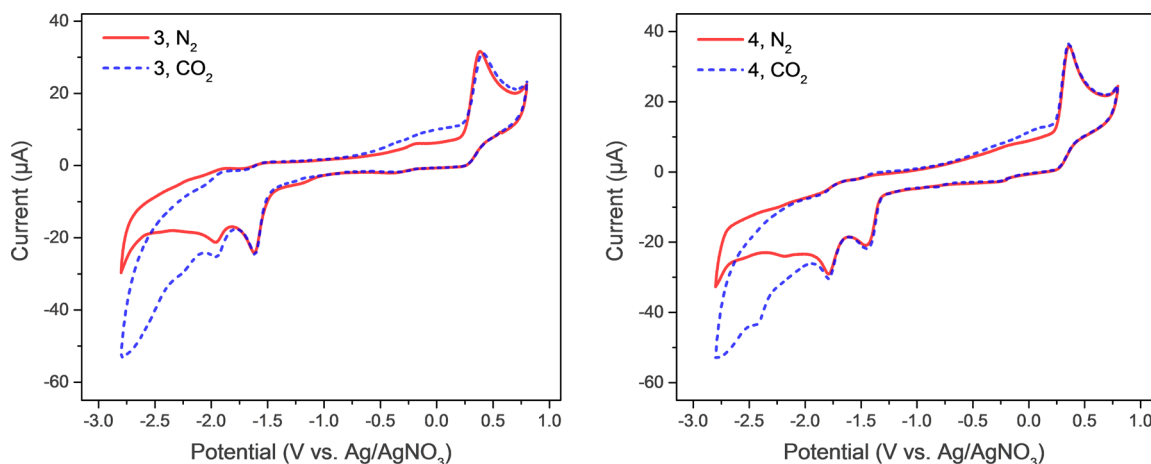

Figure 3. Cyclic voltammograms of **3** (left) and **4** (right) under N_2 and CO_2. CVs were recorded at 100 mV/s for 2 mM solutions of the complex in 0.1 M TBAPF$_6$/DMF.

linear in each case, indicating that the electroactive species diffuse freely in solution according to the Randles–Sevcik equation (see Supporting Information). These peak current values are given in Table 2.

Electrochemical Behavior in the Presence of CO_2. Upon saturating solutions of **1**–**4** with CO_2 by sparging gas for 10 min, a significant current enhancement at both cathodic waves for **1** and **2** is observed, indicative of some reactivity or interaction with CO_2. A marginal current enhancement at the second cathodic

Table 2. Electrochemical Peak Potentials for 1−4 Reported Versus Ag/AgNO₃

complex	E_{pc1} (V)	E_{pc2} (V)	E_{pc3} (V)	generated E_{pa1} (V)
1	*−1.73*[a]	*−2.28*[a]		0.50 → 0.47/0.61
2	*−1.65*[a]	*−2.13*[a]		0.57
3	−1.60	−1.92	*−2.20*[a]	
4	−1.38	−1.76		

[a]Numbers in bold and italics indicate a significant current enhancement upon addition of CO_2.

wave of **3** and little to no current enhancement at the two cathodic waves of **4** are observed. The largest contribution to the broad, ill-defined increase in current observed beyond −2.1 V for **3** and **4** is background current from direct reaction of CO_2 at the electrode surface. CVs of complexes **1** and **2** also exhibit a broad anodic feature from −0.65 to 0.50 V in the presence of CO_2 after reduction at the first or second cathodic wave, indicating the formation of a new species. This feature also obeys the Randles−Sevcik equation up to 1000 mV/s, indicating a freely diffusing species formed upon reduction of the complex. The results of controlled potential electrolysis experiments in the presence of CO_2 and a Brønsted acid source are discussed below.

DFT Modeling of Reduced Species. To better understand the state of the reduced complexes in solution, DFT modeling was employed. The model complexes **DFT-1** and **DFT-3** were geometry-optimized to stationary points in a conductor-like polarizable continuum model (CPCM) of acetonitrile. The unreduced monocationic species showed lowest unoccupied molecular orbital (LUMO) geometries primarily centered on the pyridyl ring but also containing some Pd and imidazolilydene character (Figure 4). Electrons were added to the model complexes *in silico*, and the calculated changes were observed. For **DFT-1**, the addition of one electron resulted in reduction of the pyridyl ring, causing contractions of the C2−C3 and C5−C6 bonds and corresponding expansions of the other bonds, and a slightly contracted Pd−N bond (Supporting Information, Figure S7). For **DFT-3**, the same was true to a different degree, with other parts of the conjugated ligand also being affected.

Addition of a second electron resulted in more significant structural changes. For **DFT-1**, the pyridyl ring transferred its charge to the Pd and Cl atoms and was oriented 25° out of the plane of the molecule. The Pd−N bond distance increased by about 50 pm as the pyridyl fell out of a bonding orientation, and the chloride dissociated. The M-NHC bonds remained almost unchanged. For **DFT-3**, the pyridyl moiety remained reduced but pointed 28° out of plane, moving toward a tetrahedral bonding geometry within the restraints of direct bonding to the tightly Pd-bound NHC moieties. The chloride remained bound in a pseudotetrahedral geometry with a Pd−Cl bond distance of 2.51 Å.

DFT Modeling of Interaction with CO_2. The approach of CO_2 to the reduced model complexes is a key step for reactivity, and thus the energetics of this process were investigated and compared to the behavior of the known electrocatalysts Re(bpy)(CO)₃Cl and Pd(triphosphine)$^{2+}$ (where the phosphine substituents are methyl groups). Computed structures of the active reduced species that have been found to interact with CO_2 were optimized to stationary points, and then the energy of the system was recorded as a function of varying M−CO_2 distance. The CO_2 bond angle was recorded to quantify the degree of CO_2 activation (Figure 5).

Several interesting results were observed from this method. First, the reduced models of known electrocatalysts and **DFT-1** and **DFT-3** all exhibited some degree of energetic stabilization upon approach of CO_2, whereas the unreduced species repelled CO_2. Re(bpy)(CO)₃⁻ exhibited energetic stabilization starting at an M−CO_2 distance of ∼3.0 Å and a fully activated CO_2 bond angle of 120° at 2.0 Å, consistent with the presence of strong Brønsted acids not being necessary for this catalyst; strong current enhancements are seen in the presence of CO_2 alone. Reduced species of Pd(triphos)(CH₃CN)$^{2+}$ did not experience a large stabilization, consistent with the fact that strong acids such as HBF₄ are necessary for significant CO_2 current enhancement to be observed. The one-electron reduced species of **DFT-1** showed a greater stabilizing interaction with CO_2 than Pd(triphos)(CH₃CN)$^+$ within 2.75 Å, consistent with the moderate CO_2 current enhancement observed by cyclic voltammetry, whereas the one-electron reduced species of **DFT-3** was comparable to Pd(triphos)(CH₃CN)$^+$ by this method. Each of the two-electron reduced species was stabilized by weak Pd−C bond formation with CO_2 (20 kcal/mol). **DFT-1** and **DFT-3** activated CO_2 to 137° and 139° at their respective energy minima when reduced by one electron, and both activated CO_2 to 128° when reduced by two electrons. This degree of activation suggests that, similar to the Pd(triphos)(CH₃CN)$^{2+}$ catalysts, a relatively strong acid source is required to protonate the moderately activated CO_2 adduct. Solvento species of **DFT-1** and **DFT-3** were also investigated, where the chloro ligand was replaced by an acetonitrile to see if this change affects the thermodynamics of the reaction given its importance in DuBois' triphosphine pincer catalysts, but little thermodynamic effect was evident.

Finally, in the case of Re(bpy)(CO)₃⁻ and the one-electron reduced species of **DFT-1** and **DFT-3** where the additional charge is pyridyl-centered, a charge transfer occurred from the ligand, helping to activate CO_2. This effect is very pronounced with Re(bpy)(CO)₃⁻ as can be seen in Supporting Information, Figure S7 by the significant decrease in CO_2 bond angle concomitant with a decrease in bipyridyl C2−C2′ bond length (some additional charge is transferred from the CO ligands as well, as determined by natural bond orbital charge analysis). A similar observation is also made with the one-electron reduced
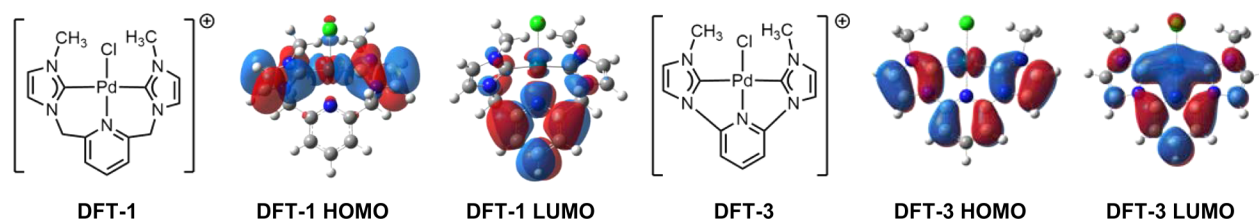
Figure 4. Structures and HOMO and LUMO orbital diagrams of **DFT-1** and **DFT-3**.
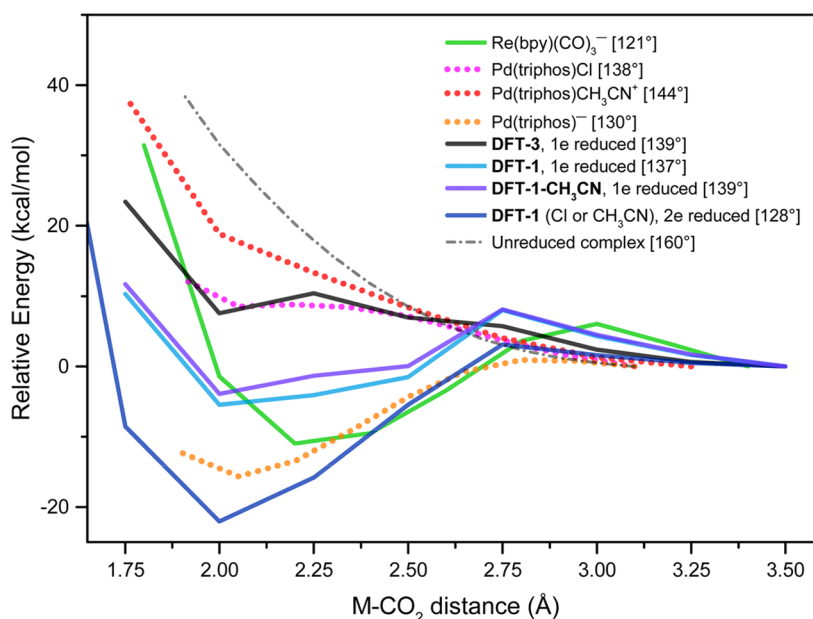
Figure 5. DFT-calculated energetics for the approach of CO_2 to a reduced complex, with CO_2 bond angles given for each energy minimum, or in the absence of a minimum, at 2.0 Å. The CPCM solvent model with acetonitrile was employed in each case. The M−CO_2 distance is measured from the metal center to the carbon of CO_2.

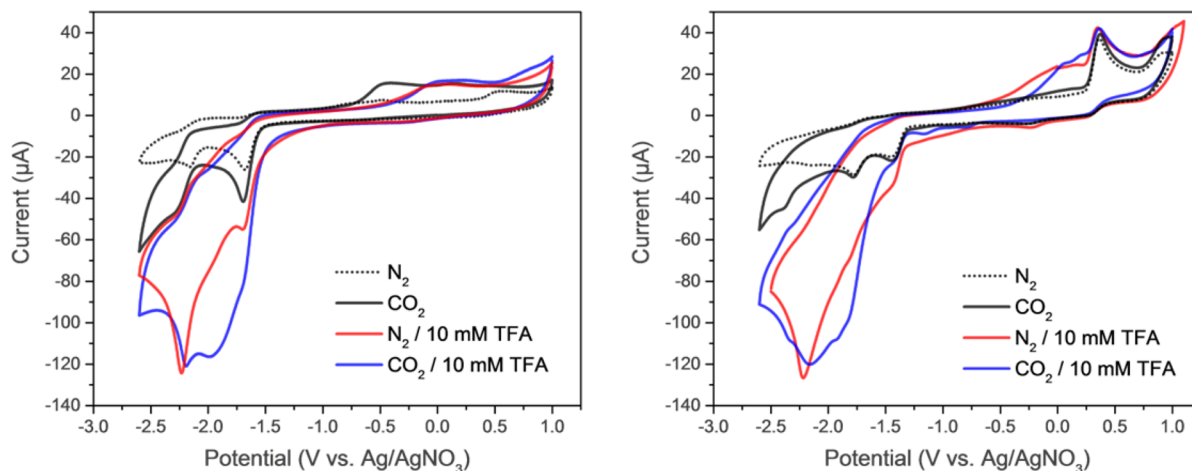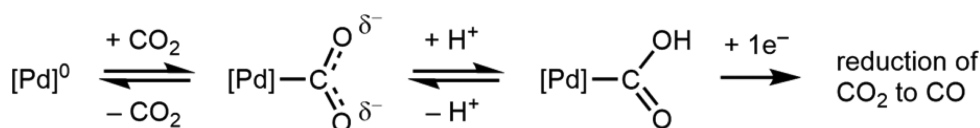**Scheme 1. Proposed Equilibria for the Protonation of Pd-Bound CO_2**

Figure 6. Cyclic voltammograms of complexes **2** (left) and **4** (right) and blank solutions under N_2 and CO_2 with and without 10 mM TFA. CVs were recorded at 100 mV/s for 2 mM solutions of the complex in 0.1 M TBAPF$_6$/DMF.

species of **DFT-1** and **DFT-3**, though this is not observed with the two-electron reduced species. In this case, the excess charge of **DFT-1** is Pd-centered, while the excess charge of **DFT-3** is delocalized throughout the complex. **DFT-1** returns to a square planar geometry as CO_2 coordinates, whereas **DFT-3** remains pseudotetrahedral.

These results support ligand charge-transfer capabilities in pincer complexes **1−4**, akin to group 7 bipyridyl tricarbonyl electrocatalysts, and suggest that the presence of a relatively strong Brønsted acid may be required for complete CO_2 activation, akin to the group 10 triphosphine electrocatalysts.

Additionally, they correlate with the degrees of electrochemical current enhancement observed in the presence of CO_2 for all species investigated.

Electrochemical Response to Brønsted Acids. The reduction of CO_2 to fuel-relevant products such as CO, CH_3OH, and CH_4 requires a proton source (Table 1). The addition of Brønsted acids of varying strengths, 2,2,2-trifluoroethanol (TFE), glacial acetic acid (GAA), and trifluoroacetic acid (TFA) (with pK_a values of 23.6, 12.3, and 3.45 in dimethyl sulfoxide (DMSO), respectively),[30] were investigated to determine if the use of weaker acids would enable the

reduction of CO_2 while safeguarding selectivity for reduction of CO_2 over H^+ by limiting the concentration of free H^+ (Scheme 1). Ideally, the proton source should be strong enough to protonate an activated CO_2 intermediate while resulting in minimum background current at potentials relevant to the complexes.

For complexes **1** and **2**, with or without CO_2 in solution, addition of up to 500 mM TFE resulted in only a small increase in current at the most negative cathodic wave and did not affect the first cathodic wave. There was a negligible response to the addition of TFE for complexes **3** and **4**, even in the presence of CO_2. This result is in contrast to electrocatalysts such as $Mn(bpy-^tBu)(CO)_3Br$ where even weak acids such as TFE lead to large current enhancements with CO_2 present.[8] The addition of acetic acid gave similar results with lower concentrations, where the addition of 10−100 mM GAA resulted in a small increase in current at the most negative cathodic wave for both **1** and **2** and a negligible increase at the first cathodic wave.

Addition of 5 equiv of TFA to a solution of **2** resulted in a large current response under both N_2 and CO_2, indicating that the complex is able to reduce H^+ ions to form H_2 (Figure 6). The current response under N_2 and CO_2 is different in each case, indicating involvement by CO_2, and it is notable that there is a large current at potentials near that of the first cathodic wave for complexes **1** and **2** only in the presence of CO_2. To determine whether the increase in current is due to CO_2 reduction or CO_2 acting as a cofactor for H^+ reduction, preparative-scale controlled potential electrolysis (CPE) experiments were performed. Note that with TFA there is background H^+ reduction at potentials relevant to **1−4** (see Supporting Information, Figure S8).

Preparative-Scale Controlled Potential Electrolysis. CO_2-saturated 0.1 M TBAPF$_6$/DMF (TBAPF$_6$ = tetrabutylammonium hexafluorophosphate) solutions containing 2 mM of complexes **1−4** were prepared in an airtight cell with frit-separated compartments for the reference electrode and counter electrode. Electrolysis was carried out in the presence of 5 equiv of TFA for complexes **1−4** and at the potentials of the first and second cathodic waves (Table 3). A typical current versus time plot is shown in Supporting Information, Figure S9.

Complexes **3** and **4** did not exhibit any significant CO production at either first or second reduction potentials. Both complexes are stable at their first reduction potential in the

presence of TFA, though once the acid concentration diminishes due to hydrogen production, a color change from bright yellow to brown is observed; a black solid eventually precipitates. Reduction at more negative potentials leads to a color change from bright to dark yellow even in the presence of TFA and to a loss of the characteristic cathodic waves for the complexes. The lack of CO production for these complexes is consistent with the observed lack of current enhancement upon addition of CO_2 (see Figure 3), as well as with the DFT scan calculations, where the original coordination sites in **DFT-3** remain locked in a pseudotetrahedral geometry even as CO_2 is forced into a bonding orientation.

In contrast, complexes **1** and **2** exhibit significant CO production upon reduction at both the first and second cathodic potentials in the presence of CO_2 and 5 equiv of TFA. After electrolysis at the first reduction potential, the headspace gas for both complexes contained approximately a 1:10 ratio of CO/H_2, corresponding to Faradaic efficiencies (FEs) of 9% and 8% for CO production from **1** and **2**, respectively, with the remaining Faradaic current producing H_2. After electrolysis at the second reduction potential, the solution containing complex **1** produced CO with 23% FE, and the solution containing complex **2** produced CO with 28% FE.

Note that with a relatively strong acid such as TFA, direct reduction of H^+ at the electrode at these potentials is non-negligible, accounting for approximately 25% of the current passed at −1.75 V and 48% of the current passed at −2.30 V in the case of **1** (see Supporting Information). Thus, for **1**, the inherent selectivity of the complex for CO_2 reduction against H^+ reduction (TFA) is approximately 12% at −1.75 V and 43% at −2.30 V. If the same ratios of background current are assumed for complex **2**, selectivities of 12% at −1.65 V and 59% at −2.20 V are obtained. The complexes exhibit stability to reduction in the presence of CO_2 and H^+, retaining well-defined, diagnostic electrochemical features after the passage of 10 C at either the first or second cathodic peak potentials, though the formation of some fine, dark precipitate is evident after reduction at the most negative potentials. Samples taken from the headspace during electrolysis gave similar ratios of H_2 to CO compared to the final headspace analysis, indicating that there is no significant induction period affecting the selectivity of H_2 and CO.

Electrolysis was also attempted with 20 mM acetic acid and 1 M TFE for complex **1** at −2.30 V where a small current enhancement was observed to see if a weaker acid source may lead to higher selectivity for CO production. The passage of 11 C yielded hydrogen and trace CO and CH_4. The complex did not substantially decompose in this process and could be regenerated by oxidation at +0.60 V. Colorimetric spot tests with chromotropic acid and methylquinaldinium were performed on the solutions[31,32] after electrolysis to test for the presence of formate, formic acid, or formaldehyde; however, none of these compounds were detected.

To ensure that the CO detected was the product of CO_2 reduction and not from other sources of carbon and oxygen present, an isotope labeling electrolysis experiment was performed on a $^{13}CO_2$-sparged solution with the headspace gas analyzed by gas chromatography-mass spectrometry (GC-MS). The only product detected was ^{13}CO, proving CO_2 is the source. Another electrolysis experiment was performed on the solution after being briefly sparged with $^{12}CO_2$, and in this case the headspace gas showed the presence of a mixture of ^{12}CO and ^{13}CO (Supporting Information, Figure S10).

Table 3. Preparative Controlled Potential Electrolysis Results from 2 mM Solutions of 1−4 in a 0.1 M TBAPF$_6$/DMF Solution[a]

complex	potential (V)	charge passed (C)	FE H$_2$ (%)	FE CO (%)
1	−1.75	13	93	9
1	−2.30	12	79	23
2	−1.65	37	89	8
2	−1.95	4.0	83	10
2	−2.20	14	64	28
3	−1.65	15	100	0
3	−2.00	13	100	0
4	−1.50	8.2	86	0
4	−2.00	6.4	81	3

[a]The 80 mL electrochemical cell employed a reticulated vitreous carbon working electrode in a compartment containing 10 mL of solution that was separated by fritted glass from the platinum mesh counter electrode compartment, which contained 5 mL of solution. Hydrogen and carbon monoxide production are given in terms of Faradaic efficiency. Potentials are reported versus Ag/AgNO$_3$.

Table 4. Preparative Controlled Potential Electrolysis Results with Cation Additives^a

solution	acid	potential (V)	charge passed (C)	FE H$_2$ (%)	FE CO (%)
1 + 50 mM K$^+$	100 mM GAA	−2.30	7.1	27	52
1 + 50 mM K$^+$	10 mM TFA	−2.30	10	51	47
1 + 50 mM K$^+$	10 mM TFA	−1.85	5.8	63	34
1 + 65 mM Mg^{2+}	10 mM TFA	−2.30	7.2	70	30
1 + 65 mM Mg^{2+}	10 mM TFA	−1.90	7.0	78	26
1 + 30% [BMIM][PF$_6$]	10 mM TFA	−2.30	10	88	7
1 + 30% [BMIM][PF$_6$]^b	10 mM TFA	−1.90	17	72	24
4 + 35 mM Mg^{2+}	10 mM TFA	−2.10	6.6	47	2
1-CH$_3$CN^b	10 mM TFA	−1.75	26	83	17

^{a}2 mM concentrations of the respective complex in 0.1 M TBAPF$_6$/DMF solutions. The 80 mL electrochemical cell employed a reticulated vitreous carbon working electrode in a compartment containing 10 mL of solution that was separated by fritted glass from the platinum mesh counter electrode compartment, which contained 5 mL of solution. Hydrogen and carbon monoxide production are given in terms of Faradaic efficiency. All potentials reported versus Ag/AgNO$_3$. ^{b}Additional 3−4 µL increments of TFA were added for every additional 5 C of charge passed. Ratio of CO/H$_2$ in headspace was tested at approximately 7 C increments and remained similar throughout electrolysis.

Effects of Additives: Organic and Alkali Ions. Though complexes **1** and **2** reduce CO$_2$ to CO in significant measure, selectivity for CO$_2$ reduction over H$^+$ reduction is mediocre, and weaker acids, though they maintain a lower concentration of free H$^+$, are not able to sufficiently protonate the putative CO$_2$-adduct intermediate to lead to CO production (Scheme 1). To try and favor CO$_2$ activation and reduction, the use of stabilizing cations was investigated as it has been shown that the presence of alkali ions can have a synergistic effect on the activation of CO$_2$ by stabilizing the negative charge on the O atoms of a partially activated CO$_2$ molecule,[33−36] and it is well-known that the presence of Mg^{2+} ions is critical for CO$_2$ reduction in the enzyme RuBisCO.[37] Additionally, imidazolium based ionic liquids have been implicated in carbon dioxide reduction chemistry.[35,38−40] Thus, the effect of the addition of KPF$_6$, Mg(ClO$_4$)$_2$, and 1-butyl-3-methylimidazolium hexafluorophosphate ([BMIM][PF$_6$]) on the electrochemical behavior of **1** was investigated.

Improved selectivity for reduction of CO$_2$ over H$^+$ was observed in the presence of K$^+$, Mg^{2+}, and [BMIM]$^+$ (Table 4). When combined in solution with complex **1** at −2.30 V, the FE for CO production increased from 23% with no additive ions to 47% with 50 mM K$^+$ and to 30% with 65 mM Mg^{2+}. In a 30% [BMIM][PF$_6$]/DMF solution (v/v), the selectivity for CO production decreased at this negative potential, perhaps due to excess stabilization of the reduced complex by the high concentration of imidazolium ions. (In [BMIM][PF$_6$], little to no decomposition was observed, even after the passage of 27 C of charge.) At the first reduction potential of **1** the greatest improvements for selectivity were observed, where the FE for CO production improved from 9% with no additive ions to 24% with [BMIM][PF$_6$], 26% with Mg^{2+}, and 34% with K$^+$. If the same amount of background H$_2$ production without the presence of these additives is assumed to occur, and this is subtracted from the total amount of H$_2$ produced, the inherent selectivity for CO$_2$ reduction by **1** increases from 12% at the first reduction potential to approximately 35% with [BMIM]$^+$ or Mg^{2+} and to 49% with K$^+$ and from 43% at the second reduction potential to approximately 58% with Mg^{2+} and to 93% with K$^+$. These results are consistent with stabilization of a CO$_2$-adduct intermediate by interaction of the cation with the negatively charged O atoms of CO$_2$, helping favor reduction of CO$_2$ over H$^+$.

Note that the presence of K$^+$ ions alone at the most negative potentials used in electrolysis (−2.30 V) resulted in some non-negligible CO production with GAA, though only trace CO was produced at −1.75 and −2.0 V (see Supporting Information,

Table S1). The presence of Mg^{2+} ions or [BMIM][PF$_6$] in solution alone did not result in any significant CO production with TFA or GAA even at −2.30 V. Finally, the presence of Mg^{2+} with complex **4** was investigated, but no changes in reactivity were observed. The pyridyl-bridged species **3** and **4** remain almost entirely selective for H$^+$ reduction.

Solvento Species. In another effort to increase selectivity for CO production the chloro ligand was replaced with a more labile acetonitrile ligand, forming a dicationic complex. It is known that a labile ligand in the fourth coordination site served an important role in the activity of Pd(triphosphine)$^{2+}$ pincer catalysts of DuBois, and reduction of a dicationic complex should occur at less negative potentials.

Solvento complexes of **1−4** were readily prepared by halide abstraction with a silver salt in acetonitrile, resulting in dicationic complexes with a labile acetonitrile ligand. ^{1}H NMR spectra of these species in DMSO-d_6 contained a singlet at δ 2.07 ppm characteristic of free acetonitrile,[41] indicating displacement by the solvent (DMSO or methanol; see Supporting Information, Figures S11 and S12), and attenuated total reflection−Fourier transform infrared (ATR-FTIR) spectra revealed nitrile stretches centered at 2342 cm^{-1} (Supporting Information, Figure S13). X-ray quality crystals of [Pd(C^N^C)(CH$_3$CN)](BF$_4$)$_2$, **1-CH$_3$CN**, were grown, unambiguously revealing the presence of a coordinated CH$_3$CN molecule (Supporting Information, Figure S14). The Pd−CH$_3$CN bond lengths were 1.978(2) and 1.999(1) Å for the disordered solvento ligand, typical for CH$_3$CN *trans* to an imine, pyridine, amine, or carbonyl donor.[42−44] CV analysis was performed on these solvento complexes. In each case, the first cathodic wave shifted anodically by a few hundred millivolts relative to the parent halide complex (Table 5). These shifted cathodic waves could also be generated by the addition of silver hexafluorophosphate to solutions of **1−4** in the electrochemical cell. Because of the presence of adventitious halide ions in the electrolyte solution and the

Table 5. Peak Potentials Versus Ag/AgNO$_3$ of the First Cathodic Wave for 1−4 and Their Acetonitrile Substituted Analogues [1−4]-CH$_3$CN

complex	E_{pc1}(Cl) (V)	E_{pc1}(CH$_3$CN) (V)	ΔE_{pc1} (V)
1	−1.73	−1.39	+0.34
2	−1.65	−1.50	+0.15
3	−1.59	−1.29	+0.30
4	−1.38	−1.17	+0.21

lability of the solvento ligand, cathodic waves for both the halide and solvento complexes were simultaneously present except immediately after *in situ* halide abstraction with silver hexafluorophosphate. Conversely, the addition of sodium chloride removed the anodically shifted waves.

Reduction of **1-CH$_3$CN** was examined in the presence of CO_2 and 10 mM TFA, showing an anodic shift from −1.75 to −1.63 V for the peak potential of the first cathodic wave upon addition of TFA (Figure 7). Electrolysis at the potential of the first wave
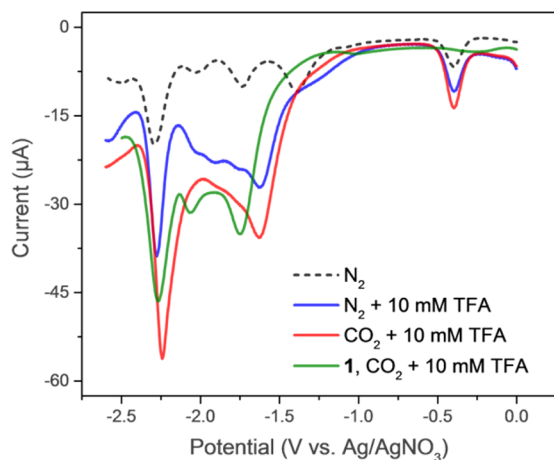

Figure 7. Square wave voltammograms of **1-CH$_3$CN** with 10 mM TFA under N$_2$ and CO_2 and of **1** with 10 mM TFA under CO_2.

resulted in CO production with 17% Faradaic efficiency, an improvement from 9% with complex **1** (Table 4). Complex **3-CH$_3$CN** was also examined (Supporting Information, Figure S15), with electrolysis at −2.0 V yielding <1% CO.

Finally, it was noticed that in contrast to complex **1**, reduction of **1-CH$_3$CN** at its first cathodic wave did not produce a corresponding anodic wave within the scanned potential range. Another complex, **1-Br**, containing a bromo ligand in place of the chloro group, was also examined and showed a corresponding anodic wave with a peak potential of 0.40 V, shifted relative to an initial peak potential of 0.50 V in **1**. This may indicate the necessity of a halide being present for formation of the reduced species, or else the reduced **1-CH$_3$CN**, being cationic, may be oxidized at a more positive potential outside the scanned range. EPR of **1-Br** after reduction indicated the presence of a species with Pd(I) character and an axially elongated square planar structure ($g(x) = 2.0075$, $g(y) = 2.0075$, $g(z) = 2.1110$). These results are comparable to those observed for both monometallic and bridged Pd(I) species in the literature.[45,46] Rotating disk electrode experiments were performed to differentiate between monometallic and bimetallic alternatives, where a bimetallic species would diffuse more slowly. The diffusion rates of the nonreduced and one-electron-reduced species were determined to be 5×10^{-6} cm^2/s and 9×10^{-6} cm^2/s, respectively, according to the Levich equation. Additionally, DFT optimizations of a putative halide-bridged dimer converged to individual mononuclear species. Thus, a mononuclear species is supported as the product in contrast to Pd(triphosphine)(CH$_3$CN)$^{2+}$, which loses activity due to the formation of a Pd(I) bridged species. The singly occupied molecular orbital (SOMO) of the one-electron-reduced species of **DFT-1** has both Pd and pyridyl character (Figure 8), and it is proposed that this ligand involvement contributes to the stability of a reduced mononuclear species,
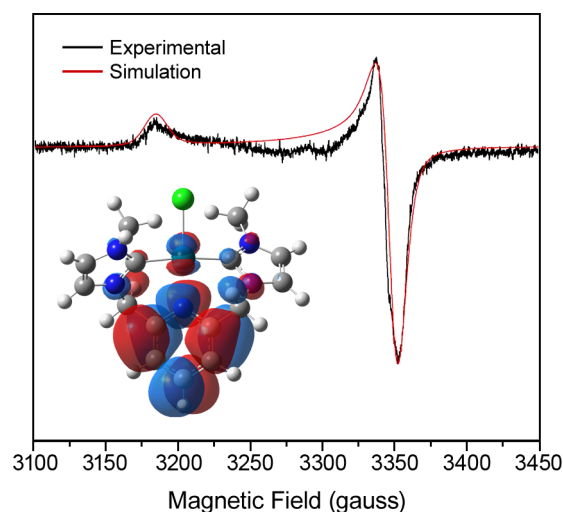

Figure 8. Experimental and simulated EPR spectra for the one-electron reduced product of **1-Br** overlaid by a stable, computed structure with SOMO geometry for one-electron-reduced **DFT-1**.

potentially resolving a major source of deactivation which occurs with triphosphine pincer complexes.

Testing for Reactivity by a Heterogeneous Species. To test whether the observed activity is authentically due to the solution species and not the result of a decomposition product being deposited on the electrode surface, the high surface area electrodes were carefully removed from solution after controlled potential electrolysis experiments had been performed with solutions initially containing complex **1**, 65 mM Mg^{2+}, and 10 mM TFA, and also **1-CH$_3$CN** and 10 mM TFA under CO_2, and then placed into new CO_2-saturated solutions containing 10 mM TFA only. No potential was applied to the electrode until the solutions were electrolyzed at −1.90 V. Only trace amounts of CO were detected (0.002−0.004% in the headspace gas) as well as 1.3% H$_2$ after the passage of 6 C, consistent with the active species being the dissolved complex and not a decomposition product deposited on the electrode surface.

Additionally, plots of peak current against the square root of the scan rate for **1−4** are linear in each case, including for the electrochemically generated anodic waves (see Supporting Information), suggesting that the electroactive species are freely diffusing in solution according to the Randles−Sevcik equation.

■ CONCLUSION

The bis-NHC palladium pincer complexes **1−4** were electrochemically characterized, with the lutidine-linked complexes **1** and **2**, which were demonstrated to electrocatalytically reduce CO_2 to CO in the presence of strong acids such as TFA. The one-electron reductions of **1** and **2** were shown to be chemically reversible and, due to charge delocalization onto the pyridyl moiety, avoid decomposition into inert bimetallic species, thereby circumventing the primary deactivation pathway limiting the TON of palladium triphosphine electrocatalysts. Computational studies of the initial interaction of CO_2 with reduced species of Re(bpy)(CO)$_3$Cl, Pd(triphosphine)(CH$_3$CN)$^{2+}$, and **DFT-1** correctly predicted the proton source requirements of the electrocatalytic systems by correlation to the degree of CO_2 activation and gave insight into charge-transfer dynamics of the electrocatalysts with CO_2. The reduced species of **DFT-1** exhibited charge transfer from the redox-active ligand to CO_2, a characteristic important to the reactivity of Re(bpy)(CO)$_3$Cl and

other related CO_2 reduction electrocatalysts. Selectivity for reduction of CO_2 over H^+ with **1** was improved by the addition of the CO_2-adduct-stabilizing cations K^+, Mg^{2+}, and $[BMIM]^+$ as well as by anodically shifting the first reduction potential of the complex by synthesis of the dicationic species **1-CH₃CN**. This work has demonstrated the capacity of lutidine-linked bis-NHC pincer complexes for CO_2 reduction electrocatalysis, expanding the palladium pincer motif to strongly electron-donating redox-active ligands. Investigations of related complexes with modified bis-NHC ligands are underway.

■ EXPERIMENTAL SECTION

General. Unless otherwise specified, all reactions were performed under nitrogen using standard Schlenk techniques, and solvents and reagents were used as received from commercial sources. *N*-butylbenzimidazole, $[BMIM][PF_6]$, pyridyl-linked bis-NHC pincer proligands, and palladium pincer halide complexes were synthesized according to literature procedures, with modifications noted below.[25−28,47,48] Potassium hexafluorophosphate (Aldrich), magnesium perchlorate (Alfa), anhydrous 99.8+% acetonitrile (Alfa), anhydrous 99.8+% *N,N*-dimethylformamide (Aldrich), and 99 atom % carbon-13 dioxide (Aldrich) were used as received for electrochemical experiments. Tetrahydrofuran was distilled from a sodium benzophenone ketyl still. Microwave syntheses were performed using a Biotage Initiator microwave system.

¹H NMR spectra were acquired using Bruker AV300 or Bruker AV400-Inverse spectrometers with chemical shifts referenced to residual solvent signals. Mass spectra were acquired using a Waters LC-MS ESI-MS. IR spectra were collected using a PerkinElmer Frontier FT-IR Spectrometer with ATR attachment. Gaseous products were analyzed using an SRI Model 8610C gas chromatograph equipped with molecular-sieve columns and dual TCD and FID detectors. Mass spectra for headspace gases were acquired using an Agilent 6890N gas chromatograph coupled with a 5975B MS detector. Crystallographic data was acquired using a Bruker X8 APEX II diffractometer with graphite monochromated Mo Kα radiation.

Electrochemistry. Electrochemical experiments were performed using a Pine AFCBP1 bipotentiostat or Metrohm Autolab PGSTAT12. Cyclic voltammetry experiments were performed in an airtight three-electrode cell with a 7 mm² glassy carbon working electrode (Bioanalytical Systems, Inc.), Pt mesh counter electrode, and Ag wire pseudoreference electrode in a 0.010 M $AgNO_3$ acetonitrile solution separated from the bulk solution by a Vycor frit. Experiments were performed under N_2 or CO_2 using 2 mM concentrations of the complexes in 10 mL of anhydrous electrolyte solution unless otherwise stated. Controlled potential experiments used reticulated vitreous carbon or glassy carbon rod working electrodes. Glassy carbon electrodes were cleaned by successive polishing with 1 μM, 0.3 μM, and 0.05 μM alumina paste, followed by rinsing with water, sonication (5 min) in distilled water, and sonication (5 min) in methanol. Reticulated vitreous carbon electrodes were cleaned by electrochemical oxidation at +1.0 V versus $Ag/AgNO_3$ followed by thorough rinsing with acetone and then methanol, resulting in a reflective carbon surface. A 5.0 mm diameter glassy carbon electrode (Pine) was used for rotating-disk electrode experiments. Electrolyte solutions were 0.1 M triply recrystallized $TBAPF_6$ in anhydrous DMF and sparged with nitrogen prior to use. Decamethylferrocene was used as an internal standard with its reversible redox couple observed at -404 ± 5 mV versus $Ag/AgNO_3$.[49] Peak potentials were determined by square wave voltammetry at 25 Hz.

Electron Paramagnetic Resonance Spectroscopy. The EPR spectrum of **1-Br** after electrochemical one-electron reduction was obtained in frozen solution at 77 K using a Bruker Elexsys E500 series continuous wave EPR. The spectrometer was operated at a frequency of 9.40 GHz (X-band) with 50 kHz field modulation and 8G modulation amplitude.

Computational Methods. DFT calculations were performed using Gaussian 09 (Revision D.01) using the long-range and dispersion-corrected ωB97xD hybrid functional.[50] The D95(d) basis set was used for all atoms except palladium, which employed the Stuttgart-Dresden-Bonn quasi-relativistic effective-core potential and corresponding correlation-consistent triple-ζ basis set.[51,52] Frequency calculations were performed on all geometry-optimized structures to ensure that energy minima were achieved.

Synthesis. *2,6-Bis(3-butylbenzimidazol-1-ium)pyridine dibromide, BzCNBzC-Bu·2Br.* This compound was prepared via a procedure that was modified from the literature.[28] Benzimidazole (4.23 mmol, 500 mg), 2,6-dibromopyridine (1.92 mmol, 456 mg), and K_2CO_3 (4.23 mmol, 585 mg) were heated together without solvent at 185 °C for 2 h and then at 160 °C for 30 h. When this mixture cooled, a white solid formed, which was ground into a powder and washed with water and Et_2O. The powder was taken up in DMF (7 mL), and an excess of 1-bromobutane (3 mL) was added. The mixture was heated to 100 °C, and the resulting solution was left to stir overnight, resulting in the formation of a white precipitate. When the mixture cooled, the powder was washed with diethyl ether (25 mL × 2), collected by centrifugation, and dried under vacuum yielding an off-white powder (595 mg, 53.4% yield). ¹H NMR $((CD_3)_2SO)$, 400 MHz): δ ppm 0.99 (t, J = 7.39 Hz, 6 H), 1.48 (sxt, J = 7.46 Hz, 4 H), 2.04 (quin, J = 7.46 Hz, 4 H), 4.69 (t, J = 7.23 Hz, 4 H), 7.74 (t, J = 7.61 Hz, 2 H), 7.82 (t, J = 7.54 Hz, 2 H), 8.30 (d, J = 8.22 Hz, 2 H), 8.37 (m, J = 8.07 Hz, 2 H), 8.46 (m, J = 8.38 Hz, 2 H), 8.77 (t, J = 8.07 Hz, 1 H), 10.81 (s, 2 H)

1-Br, [Pd(C^N^C-Bu)Br](PF₆). A dark red-orange solution of C^N^C-Bu·2Br (0.44 mmol, 228 mg) and $Pd(OAc)_2$ (0.44 mmol, 100 mg) in 3.5 mL of DMSO was left to stir under vacuum for 1 h at room temperature, then blanketed with N_2. The solution was then reacted in a microwave at 160 °C for 30 min (40 W). The resulting dark yellow mixture was filtered to remove a black solid, with the solvent removed under vacuum at 60 °C. The bright orange residue was taken up in a minimum of dichloromethane and added dropwise to diethyl ether (12 mL), resulting in the formation of a light orange solid. This process was repeated, and the product was then purified by column chromatography over SiO_2 using an 85:10:5 (v/v) acetonitrile/water/saturated KNO_3(aq) eluent. The eluted product was taken up in methanol, filtered, concentrated to dryness, and reacted with 3 equiv of NH_4PF_6 in acetonitrile. The solvent was removed, and the residue was taken up in dichloromethane and washed with water, with the dichloromethane extracts concentrated and added dropwise to diethyl ether, resulting in the formation of a light orange solid (106.5 mg, 35% yield). ¹H NMR $((CD_3)_2SO$, 300 MHz): δ ppm 0.88 (t, J = 7.31 Hz, 7 H), 1.16−1.33 (m, 5 H), 1.70−1.87 (m, 4 H), 4.17−4.33 (m, 2 H), 4.42−4.57 (m, 2 H), 5.54−5.72 (m, 4 H), 7.44 (d, J = 1.60 Hz, 2 H), 7.59 (d, J = 1.48 Hz, 2 H), 7.85 (d, J = 7.77 Hz, 2 H), 8.21 (t, J = 7.71 Hz, 1 H) ESI-MS $[M-Br]^+$ = 538.2 m/z

General Synthesis Method for Solvento Complexes. Acetonitrile-bound complexes were prepared by addition of 1.1 equiv of $AgBF_4$ to stirring solutions of $[Pd(CNC)X](Y)$ (where CNC is a lutidine- or pyridine-linked bis-NHC pincer ligand, X = Cl, Br, and Y = BF_4, Br) complexes in dry acetonitrile in the absence of light. After they stirred for 1 h at room temperature, the mixtures were centrifuged to remove a gray powder and then filtered through Celite, with the resulting solution concentrated to saturation and added dropwise to 10 mL of Et_2O resulting in the formation of a pale yellow precipitate. The hygroscopic powders were isolated and dried under vacuum at 40 °C overnight.

1-CH₃CN, [Pd(C^N^C)(CH₃CN)](BF₄)₂. Pale yellow hygroscopic powder (119.7 mg, 93% yield). X-ray quality crystals grown by slow diffusion of Et_2O into a saturated CH_2Cl_2/CH_3CN solution of 7 at −30 °C. ¹H NMR $((CD_3)_2SO)$, 400 MHz): δ ppm 0.89 (t, J = 7.35 Hz, 6 H), 1.17−1.36 (m, 4 H), 1.75−1.87 (m, 4 H), 2.07 (s, 3 H), 4.09−4.26 (m, 4 H), 5.69 (d, J = 15.19 Hz, 2 H), 5.86 (d, J = 15.03 Hz, 2 H), 7.48−7.56 (m, 2 H), 7.66 (d, J = 1.49 Hz, 2 H), 7.84 (d, J = 7.76 Hz, 2 H), 8.22 (t, J = 7.68 Hz, 1 H) ESI-MS $[M−2BF_4−CH_3CN+Cl]^+$ = 494.3 m/z.

2-CH₃CN, [Pd(bC^N^bC)(CH₃CN)](BF₄)₂. Orange-brown hygroscopic powder (83.2 mg, 77% yield). ¹H NMR $((CD_3)_2SO)$, 400 MHz): δ ppm 0.90 (t, J = 7.31 Hz, 6 H), 1.27 (q, J = 7.20 Hz, 2 H), 1.37−1.53 (m, 2 H), 1.81−2.01 (m, 4 H), 2.07 (s, 3 H), 4.44−4.72 (m, 4 H), 6.03 (d, J = 15.23 Hz, 2 H), 6.30 (d, J = 15.23 Hz, 2 H), 7.44−7.66 (m, 8 H), 7.93 (d, J = 8.22 Hz, 2 H), 8.04 (d, J = 7.92 Hz, 2 H), 8.13 (d, J = 8.22

Hz, 2 H), 8.24 (t, J = 7.77 Hz, 1 H) ESI-MS [M−2BF$_4$−CH$_3$CN+Cl]$^+$ = 592.1 m/z.

3-CH$_3$CN, [Pd(C-N-C)(CH$_3$CN)](BF$_4$)$_2$. Yellow hygroscopic powder (80.2 mg, 82% yield). ^{1}H NMR ((CD$_3$)$_2$SO, 400 MHz): δ ppm 0.94 (t, J = 7.16 Hz, 6 H), 1.34 (m, J = 7.50, 4 H), 1.76−1.90 (m, 4 H), 2.08 (s, 3H), 4.22 (t, J = 6.85 Hz, 4 H), 7.86 (s, 2 H), 8.03 (d, J = 8.53 Hz, 2 H), 8.50 (s, 2 H), 8.62 (t, J = 8.38 Hz, 1 H) ESI-MS [M−2BF$_4$−CH$_3$CN +Cl]$^+$ = 466.2 m/z.

4-CH$_3$CN, [Pd(bC-N-bC)(CH$_3$CN)](BF$_4$)$_2$. Beige hygroscopic powder (68.0 mg, 70% yield). ^{1}H NMR ((CD$_3$)$_2$SO, 400 MHz): δ ppm 0.96 (t, J = 7.27 Hz, 6 H), 1.39−1.51 (m, 4 H), 1.90−2.01 (m, 4 H), 2.08 (s, 3 H), 4.64−4.74 (m, 4 H), 7.70−7.81 (m, 4 H), 8.18 (d, J = 7.60 Hz, 2 H), 8.49 (d, J = 8.26 Hz, 2 H), 8.56 (d, J = 7.76 Hz, 2 H), 8.69 (t, J = 8.10 Hz, 1 H) ESI-MS [M−2BF$_4$−CH$_3$CN+Cl]$^+$ = 566.1 m/z.

■ ASSOCIATED CONTENT

ⓢ Supporting Information

^{1}H NMR spectra and square wave voltammograms of **1**−**4**, CPE data from control samples without any complex present, crystallography data, rotating-disk electrode voltammetry data for **1**-**Br**, and plots of i_p vs $\nu^{1/2}$ for **1**−**4**. This material is available free of charge via the Internet at http://pubs.acs.org.

■ AUTHOR INFORMATION

Corresponding Author

*E-mail: mwolf@chem.ubc.ca. Phone: (604) 822-1702. Fax: (604) 822-2847.

Notes

The authors declare no competing financial interest.

■ ACKNOWLEDGMENTS

■ REFERENCES

(1) Benson, E. E.; Kubiak, C. P.; Sathrum, A. J.; Smieja, J. M. *Chem. Soc. Rev.* **2009**, *38*, 89.

(2) Rakowski DuBois, M.; DuBois, D. L. *Acc. Chem. Res.* **2009**, *42*, 1974.

(3) Mikkelsen, M.; Jørgensen, M.; Krebs, F. C. *Energy Environ. Sci.* **2010**, *3*, 43.

(4) Smieja, J. M.; Kubiak, C. P. *Inorg. Chem.* **2010**, *49*, 9283.

(5) Overett, M. J.; Hill, R. O.; Moss, J. R. *Coord. Chem. Rev.* **2000**, *206−207*, 581.

(6) Appel, A. M.; Bercaw, J. E.; Bocarsly, A. B.; Dobbek, H.; DuBois, D. L.; Dupuis, M.; Ferry, J. G.; Fujita, E.; Hille, R.; Kenis, P. J. A.; Kerfeld, C. A.; Morris, R. H.; Peden, C. H. F.; Portis, A. R.; Ragsdale, S. W.; Rauchfuss, T. B.; Reek, J. N. H.; Seefeldt, L. C.; Thauer, R. K.; Waldrop, G. L. *Chem. Rev.* **2013**, *113*, 6621.

(7) Hawecker, J.; Lehn, J.-M.; Ziessel, R. *J. Chem. Soc., Chem. Commun.* **1984**, *984*, 328.

(8) Smieja, J. M.; Sampson, M. D.; Grice, K. A.; Benson, E. E.; Froehlich, J. D.; Kubiak, C. P. *Inorg. Chem.* **2013**, *52*, 2484.

(9) Sampson, M. D.; Nguyen, A. D.; Grice, K. A.; Moore, C. E.; Rheingold, A. L.; Kubiak, C. P. *J. Am. Chem. Soc.* **2014**, *136*, 5460.

(10) Agarwal, J.; Shaw, T. W.; Stanton, C. J.; Majetich, G. F.; Bocarsly, A. B.; Schaefer, H. F. *Angew. Chem., Int. Ed.* **2014**, *53*, 5152.

(11) Costentin, C.; Drouet, S.; Robert, M.; Savéant, J.-M. *J. Am. Chem. Soc.* **2012**, *134*, 11235.

(12) Thoi, V. S.; Chang, C. J. *Chem. Commun.* **2011**, *47*, 6578.

(13) Thoi, V. S.; Kornienko, N.; Margarit, C. G.; Yang, P.; Chang, C. J. *J. Am. Chem. Soc.* **2013**, *135*, 14413.

(14) Savéant, J.-M. *Chem. Rev.* **2008**, *108*, 2348.

(15) Keith, J. A.; Grice, K. A.; Kubiak, C. P.; Carter, E. A. *J. Am. Chem. Soc.* **2013**, *135*, 15823.

(16) DuBois, D. L.; Miedaner, A.; Haltiwanger, R. C. *J. Am. Chem. Soc.* **1991**, *113*, 8753.

(17) DuBois, D. L.; Miedaner, A. *J. Am. Chem. Soc.* **1987**, *109*, 113.

(18) Steffey, B. D.; Curtis, C. J.; DuBois, D. L. *Organometallics* **1995**, *14*, 4937.

(19) Miedaner, A.; Noll, B. C.; DuBois, D. L. *Organometallics* **1997**, *16*, 5779.

(20) Slater, S.; Wagenknecht, J. H. *J. Am. Chem. Soc.* **1984**, *106*, 5367.

(21) Dubois, D. L. *Comments Inorg. Chem.* **1997**, *19*, 307.

(22) Fantasia, S.; Petersen, J. L.; Jacobsen, H.; Cavallo, L.; Nolan, S. P. *Organometallics* **2007**, *26*, 5880.

(23) Jacobsen, H.; Correa, A.; Poater, A.; Costabile, C.; Cavallo, L. *Coord. Chem. Rev.* **2009**, *253*, 687.

(24) Yu, R. P.; Darmon, J. M.; Milsmann, C.; Margulieux, G. W.; Stieber, S. C. E.; DeBeer, S.; Chirik, P. J. *J. Am. Chem. Soc.* **2013**, *135*, 13168.

(25) Hahn, F. E.; Jahnke, M. C.; Gomez-Benitez, V.; Morales-Morales, D.; Pape, T. *Organometallics* **2005**, *24*, 6458.

(26) Tu, T.; Malineni, J.; Dötz, K. H. *Adv. Synth. Catal.* **2008**, *350*, 1791.

(27) Danopoulos, A. A.; Tulloch, A. A. D.; Winston, S.; Eastham, G.; Hursthouse, M. B. *Dalton Trans.* **2003**, 1009.

(28) Brown, D. H.; Nealon, G. L.; Simpson, P. V.; Skelton, B. W.; Wang, Z. *Organometallics* **2009**, *28*, 1965.

(29) Schneider, J.; Jia, H.; Muckerman, J. T.; Fujita, E. *Chem. Soc. Rev.* **2012**, *41*, 2036.

(30) Bordwell, F. G. *Acc. Chem. Res.* **1988**, *21*, 456.

(31) Feigl, F.; Anger, V. *Spot Tests in Organic Analysis, 7th ed.*; Elsevier Science: Amsterdam, 1966; p 451.

(32) Aranaa, C.; Keshavarzb, M.; Pottsb, K. T.; Abrufia, H. D. *Inorg. Chim. Acta* **1994**, *225*, 285.

(33) Bhugun, I.; Lexa, D.; Savéant, J.-M. *J. Phys. Chem.* **1996**, *100*, 19981.

(34) Schmidt, M. H.; Miskelly, G. M.; Lewis, N. S. *J. Am. Chem. Soc.* **1990**, *112*, 3420.

(35) Thorson, M. R.; Siil, K. I.; Kenis, P. J. a. *J. Electrochem. Soc.* **2012**, *160*, F69.

(36) Gambarotta, S.; Arena, F.; Floriani, C.; Zanazzi, P. F. *J. Am. Chem. Soc.* **1982**, *104*, 5082.

(37) Lorimer, G. H. *J. Biol. Chem.* **1979**, *254*, 5599.

(38) Rosen, B. A.; Salehi-khojin, A.; Thorson, M. R.; Zhu, W.; Whipple, D. T.; Kenis, P. J. A.; Masel, R. I. *Science* **2011**, *334*, 643.

(39) Medina-Ramos, J.; Dimeglio, J. L.; Rosenthal, J. *J. Am. Chem. Soc.* **2014**, *136*, 8361.

(40) Rizzuto, A. M.; Pennington, R. L.; Sienerth, K. D. *Electrochim. Acta* **2011**, *56*, 5003.

(41) Fulmer, G. R.; Miller, A. J. M.; Sherden, N. H.; Gottlieb, H. E.; Nudelman, A.; Stoltz, B. M.; Bercaw, J. E.; Goldberg, K. I. *Organometallics* **2010**, *29*, 2176.

(42) Rauf, W.; Thompson, A. L.; Brown, J. M. *Dalton Trans.* **2010**, *39*, 10414.

(43) Lee, J.-J.; Yang, F.-Z.; Lin, Y.-F.; Chang, Y.-C.; Yu, K.-H.; Chang, M.-C.; Lee, G.-H.; Liu, Y.-H.; Wang, Y.; Liu, S.-T.; Chen, J.-T. *Dalton Trans.* **2008**, 5945.

(44) Das, S.; Pal, S. *J. Organomet. Chem.* **2004**, *689*, 352.

(45) Armbruster, F.; Augenstein, T.; Oña-Burgos, P.; Breher, F. *Chem.—Eur. J.* **2013**, *19*, 17899.

(46) Dai, W.; Chalkley, M. J.; Brudvig, G. W.; Hazari, N.; Melvin, P. R.; Pokhrel, R.; Takase, M. K. *Organometallics* **2013**, *32*, 5114.

(47) Milen, M.; Grün, A.; Bálint, E.; Dancsó, A.; Keglevich, G. *Synth. Commun.* **2010**, *40*, 2291.

(48) Bonhôte, P.; Dias, A.-P.; Papageorgiou, N.; Kalyanasundaram, K.; Grätzel, M. *Inorg. Chem.* **1996**, *35*, 1168.

(49) Aranzaes, J. R.; Daniel, M.; Astruc, D. *Can. J. Chem.* **2006**, *84*, 288.

(50) Chai, J.-D.; Head-Gordon, M. *Phys. Chem. Chem. Phys.* **2008**, *10*, 6615.

(51) Martin, J. M. L.; Sundermann, A. *J. Chem. Phys.* **2001**, *114*, 3408.

(52) Andrae, D.; Häußermann, U.; Dolg, M.; Stoll, H.; Preuß, H. *Theor. Chim. Acta* **1990**, *77*, 123.

12972

dx.doi.org/10.1021/ic502056w | *Inorg. Chem.* 2014, 53, 12962−12972